Journal of Modern Optics

ISSN: 0950-0340 (Print) 1362-3044 (Online) Journal homepage: http://www.tandfonline.com/loi/tmop20

Transmission characteristics of surface plasmon polaritons through a metallic rectangle above a metallic film

Haiqing Wang, Yongkai Wang, Guian Li & Zhongyue Zhang

To cite this article: Haiqing Wang, Yongkai Wang, Guian Li & Zhongyue Zhang (2016) Transmission characteristics of surface plasmon polaritons through a metallic rectangle above a metallic film, Journal of Modern Optics, 63:5, 411-416, DOI: 10.1080/09500340.2015.1076897

To link to this article: http://dx.doi.org/10.1080/09500340.2015.1076897

Published online: 24 Aug 2015.

Journal of Modern Optics, 2016
Vol. 63, No. 5, 411–416, http://dx.doi.org/10.1080/09500340.2015.1076897

Taylor & Francis
Taylor & Francis Group

Transmission characteristics of surface plasmon polaritons through a metallic rectangle above a metallic film

Haiqing Wang, Yongkai Wang, Guian Li and Zhongyue Zhang*

School of Physics and Information Technology, Shaanxi Normal University, Xi'an, China

(*Received 22 March 2015; accepted 22 July 2015*)

The effects of a silver rectangle on the transmission characteristics of surface plasmon polaritons (SPPs) that propagate at the air–silver interface are investigated using the finite-element method. Results show that the structural parameters of the rectangle and distance between rectangle and film significantly influence SPP-transmission characteristics. These effects are due to the restriction of SPPs at the air–silver interface and resonance around the rectangle.

Keywords: surface plasmon polaritons; localized surface plasmon; waveguide; plasmonics; nanophotonics; finite-element method

1. Introduction

Surface plasmon polaritons (SPPs) are surface electromagnetic waves of collective electron oscillations induced by the coupling of light with surface charges, propagating along a metal–dielectric interface, and exponentially decaying into neighboring media [1–9]. Given that SPPs can spatially confine light well beyond the diffraction limit, SPPs can be a potential key element in the future high-capacity photonic circuits. SPPs have also been extensively applied in other fields, such as metamaterials [10,11], sensors [12], and modulators [13].

The propagation characteristics of SPPs on different nanostructures have a significant function in the applications of SPP waveguides or SPP components. To date, numerous results have been reported about the propagation characteristics of SPPs along nanowires [14–16], compact periodic grooves and ridges [17,18], metal stripes [19,20], and cylindrical surface [21]. Fundamentally, the propagation characteristics of SPPs on metallic films with different topological shapes are important for their usages [22–25]. Researchers have investigated the propagation characteristics of SPPs on rough surfaces [26], flat semi-infinite interfaces [27–29], and films with hole arrays [30–32]. For surfaces with defects (protuberances or indentations), the defects function as so-called plasmon mirrors and flashlights [33,34]. For surfaces with corrugations or protrusions, the surface can couple more light, and the corrugations or protrusions can have strong electric fields around them. In addition, the propagation characteristics of SPPs on a rough surface are more sensitive to the surrounding media than those on a flat surface. Thus, the propagation characteristics of SPPs on surfaces are associated with roughness measurement, nonlinear optical property enhancement, and biosensors.

When specific metallic structures are located closely above a metallic film, the propagation characteristics of SPPs on the film are affected. In this study, the effects of a silver rectangle on the transmission characteristics of SPPs at the air–silver interface are investigated using the finite-element method. Results show obvious changes in steady-state electric-field distributions and propagation loss relative to those on a flat film. These results can be attributed to the restriction [35] and resonance [36,37] of SPPs in the resonator formed by the rectangle and film. In this work, effects of the structural parameters of the rectangle and the separation between rectangle and film on transmission properties are investigated. In our study, strong localized electric fields form around the rectangle or at the space between rectangle and film. The improved localized electric field can be used for enhanced nonlinear optics [38]. The transmission characteristics of the proposed structure can also help deliver SPPs to the film.

2. Structure and calculation method

Figure 1 illustrates the proposed structure, i.e., a silver rectangle above a semi-finite silver substrate. The width and height of the silver rectangle are a and b, respectively. The distance between rectangle and interface is d. The excitation wavelength is 0.532 μm in a vacuum. The effective index of the SPPs that propagate along the air–film interface is obtained using the mode analysis of the finite-element method software COMSOL Multiphysics

*Corresponding author. Email: zyzhang@snnu.edu.cn

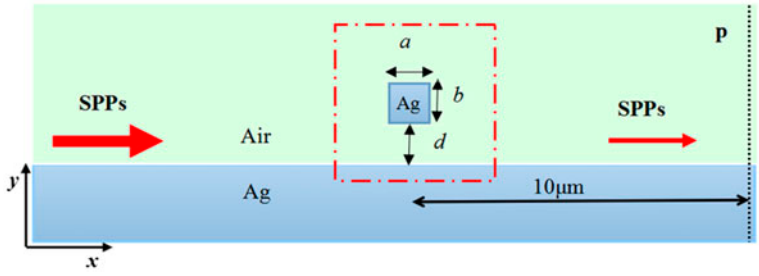

Figure 1. Schematic of SPPs propagation along the interface of air and silver film. A silver rectangle is located above the film. (The color version of this figure is included in the online version of the journal.)

4.3. A two-dimensional structure composed of a rectangle and metallic film is proposed. The perfect matching layers are set as boundary conditions, and the minimum grid size used in all calculations is 0.2 nm. Steady-state electric-field distributions and transmittance coefficients are used to study the effects of silver rectangle on the transmission characteristics of SPPs on metallic film using COMSOL Multiphysics. The magnitude of total electric field is used in the steady-state electric-field distributions. We set two ports at which the SPPs are sequentially excited and received in COMSOL Multiphysics to calculate transmittance, which corresponds to the "S_{21}" element in the scattering matrix [39]. Transmittance coefficients are defined as $T = S/S_0$, where S is the power flow over location P (a plane set at a distance of 10 μm away from the center of rectangle) of film with rectangle, and S_0 is the power flow over the location P of film without the rectangle. Thus, ohmic loss along the propagation direction at the air–silver interface can be neglected. When power flow through location P is calculated, the integral is from the film to the height at which the electric field drops to $1/e$. The complex refractive index of silver is adopted from Ref. [40].

When the excitation wavelength is equal to 0.532 μm, the effective refractive index of the SPPs on the flat silver film is 1.0452 – 0.0015i, which is calculated using the mode analysis of COMSOL software. Thus, the wavelength of SPPs is 0.509 μm, and the propagation length is 27.735 μm. The effective refractive index is set at the input port, which is 2 μm away from the center of the rectangle and can generate propagating SPPs with wavelength $\lambda_0 = 0.509$ μm at the film. The electric field of the SPPs is TM polarized and exponentially decays from the surface [1]. Given the large propagation loss of electromagnetic wave in the metal, the electric-field amplitudes decay faster (exponential attenuation constant $\alpha = 3.971 \times 10^7\ \mathrm{m}^{-1}$) than those in air (exponential attenuation constant $\alpha = 3.886 \times 10^6\ \mathrm{m}^{-1}$). Thus, electric-field intensity decays in the form $\exp(-\alpha x)$ and the energy intensity decays as $\exp(-2\alpha x)$, where x is penetration length in air.

3. Results and discussion

3.1. *Effect of distance* d *between rectangle and film on transmission*

To determine the effect of distance d between rectangle and film on the transmission characteristics of SPPs, the transmittance coefficients of the proposed structure are calculated with different d values from 0 nm to 200 nm at $a = b = 20$, 40, 60, 80, and 100 nm. As shown in Figure 2(a), a transmittance valley can be observed at approximately $d = 5$ nm. With further increased d beyond 5 nm, transmittance coefficients rapidly increase. When d is > 100 nm, transmittance coefficients do not vary significantly with increased d. In addition, the proposed structure with a large a or b ($a = b$) generates small transmittance.

To understand the mechanism in Figure 2(a), the steady-state electric-field distributions for different values of distance d at $a = b = 60$ nm are calculated. Figure 2(b) shows the plot of the steady-state electric-field distribution of the proposed structure at $d = 0$ nm. A strong electric field occurs on the left side of the rectangle and many SPPs are reflected back. Figure 2(c) plots the steady-state electric-field distribution of the proposed structure at $d = 6$ nm, which corresponds to the valley of transmittance spectrum in Figure 2(a). A strong electric field occurs in the space between rectangle and film. When SPPs transmit the rectangle, SPPs propagate not only from the top surface of the rectangle but also from the space between rectangle and film. The wavelength of SPPs on the top surface of the rectangle and its wave vector are the same as those at the film, i.e., $\lambda_0 = 0.509$ μm and $k_0 = 2\pi/\lambda_0$, respectively. The wavelength λ_1 of SPPs between rectangle and film strongly depends on the distance between them. Transmission peaks or valleys are due to the relation

$$2a = N \bullet \lambda_1/2 \ = \ \pi/(k_1) \bullet N, \qquad (1)$$

where N is an integer. The transmission peak occurs when N is even and the valley has an odd N value. For example, at the peak of $a = b = 100$ nm and $d = 4$ nm in Figure 2(a),

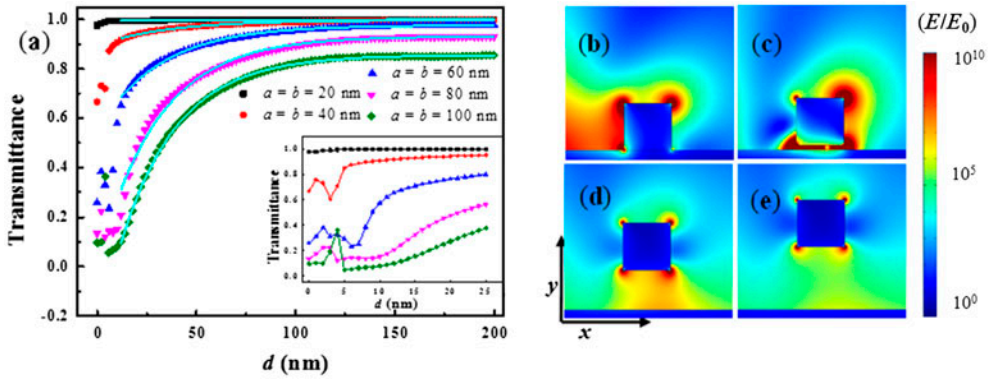

Figure 2. (*a*) Calculated transmittances of the proposed structure with different d values for different $a = b$. The inset represents the transmittance for d ranging from 0 nm to 25 nm with higher resolution. The cyan solid lines are the fitting using Equation (3) from $d = 12$ nm to $d = 200$ nm. (*b*)–(*e*) Steady-state electric-field distributions of the proposed structure for $a = b = 60$ nm at different d values: (*b*) $d = 0$ nm, (*c*) $d = 6$ nm, (*d*) $d = 30$ nm, and (*e*) $d = 80$ nm. (The color version of this figure is included in the online version of the journal.)

the corresponding effective index and SPP wavelength are $n_1 = 4.6760 - 0.0847i$ and $\lambda_1 = 0.114$ μm. Thus, $N = 4$, which satisfies Equation (1). Figure 2(*d*) and (*e*) shows the steady-state electric-field distribution of the proposed structure at $d = 30$ nm and $d = 80$ nm, respectively. A strong electric field occurs not only in the space between rectangle and film but also around the rectangle.

The above descriptions indicate that the energy of SPPs that contributes to transmittance is mainly energy transmitted from the space between rectangle and substrate. If the silver rectangle approaches the substrate, the decay rate of the electric field in air would differ from that without the rectangle. Thus, factor t is introduced, and the energy intensity decays as a function of exp $(-2t\alpha)$. The Poynting vector S transmitted from the space between rectangle and film is

$$S = \int_0^d E_0^2 \exp(-2t\alpha x)dx = E_0^2 \frac{1-\exp(-2t\alpha d)}{2t\alpha}, \qquad (2)$$

where E_0 is the electric-field intensity on the surface of film without rectangle. Transmittance as a function of the space distance d is

$$\begin{aligned} T &= \frac{S}{S_0} + B = \frac{E_0^2}{S_0}\frac{1-\exp(-2t\alpha d)}{2t\alpha} + B \\ &= A\frac{1-\exp(-2t\alpha d)}{t} + B, \quad A = \frac{E_0^2}{2S_0\alpha}, \end{aligned} \qquad (3)$$

where A is a constant parameter associated with the incident field. The scattering electric field couples with the electric field of SPPs propagating at the film, which affects the magnitude of the SPP electric field and the transmittance. We ascribe the scattering effect to B as a compensation factor. The cyan curves from $d = 12$ nm in Figure 2 are the fitting of the transmittance coefficients

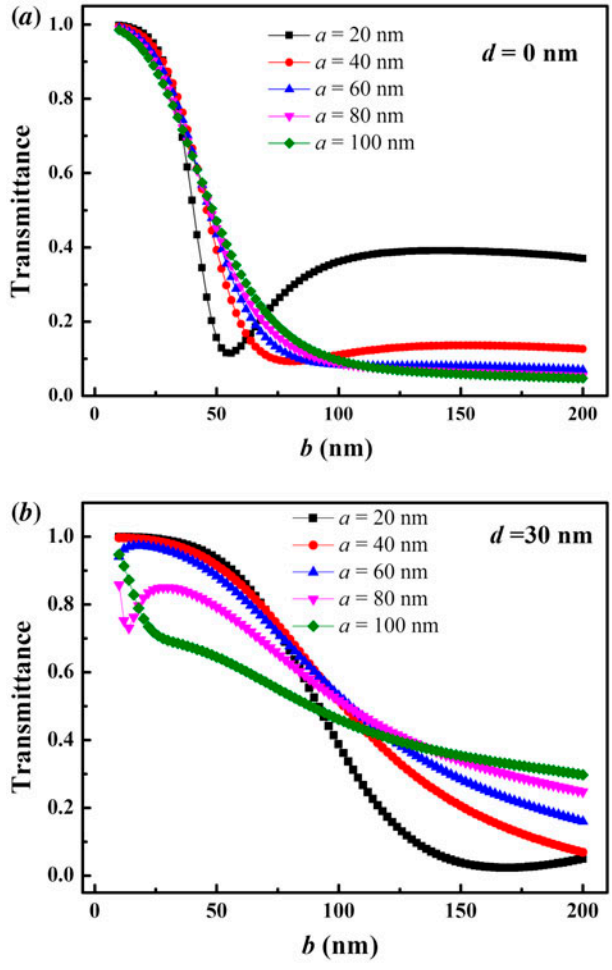

Figure 3. Calculated transmittances of the proposed structure for different a as a function of b with (*a*) $d = 0$ nm, (*b*) $d = 30$ nm. (The color version of this figure is included in the online version of the journal.)

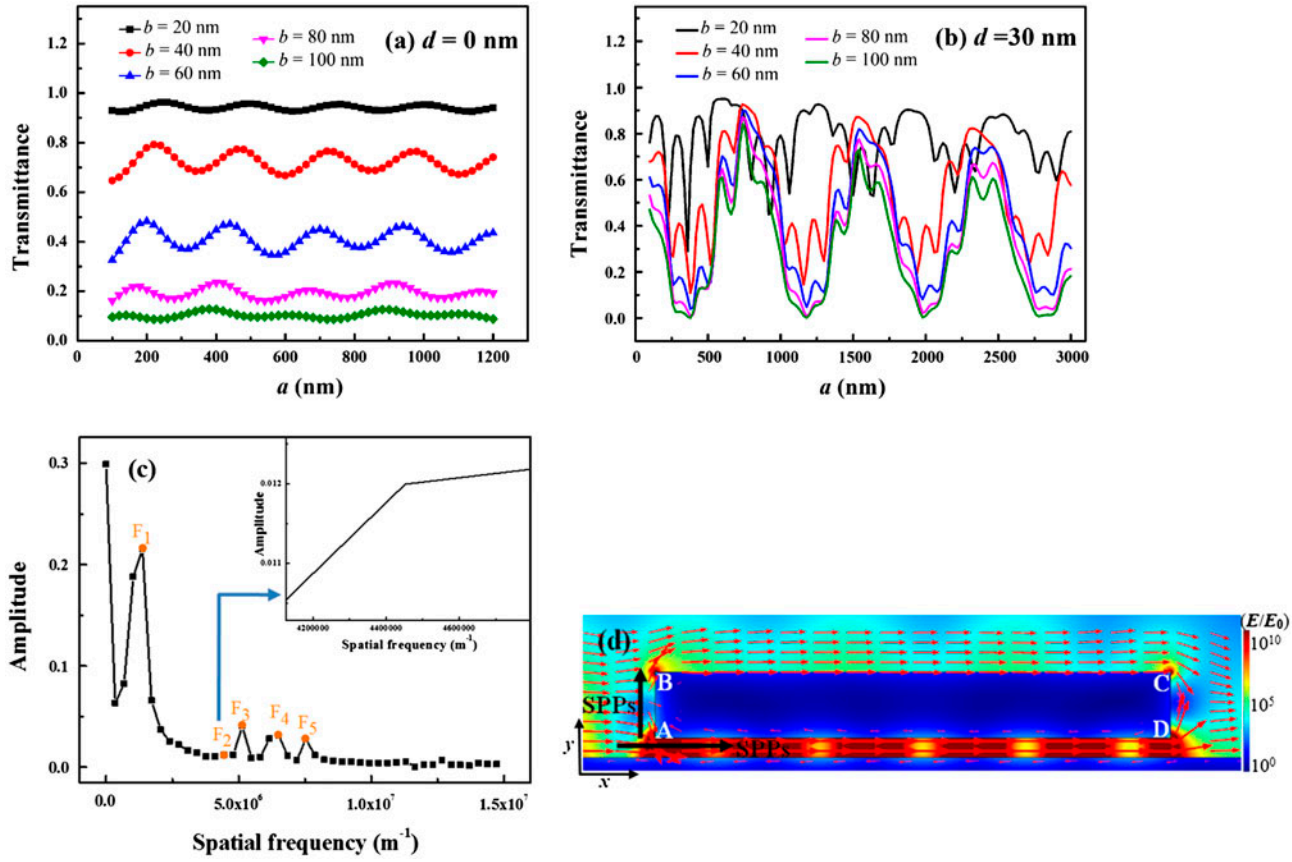

Figure 4. Calculated transmittances of the proposed structure for different b as a function of a with (a) $d = 0$ nm, (b) $d = 30$ nm. (c) The Fourier transform for $b = 100$ nm with $d = 30$ nm. (d) Distributions of steady-state electric field (color bar) and energy flow (red arrows) at $a = 780$ nm and $b = 100$ nm with $d = 30$ nm. (The color version of this figure is included in the online version of the journal.)

using Equation (3), which agree with the transmittance from numerical calculations. We fit the curve from $d = 12$ nm, which guarantees decay of the electric field away from the metallic surface and that the analytical model can fit the transmittances well with different d values. When a and b increase from $a = b = 20$ nm to $a = b = 100$ nm, t monotonically increases from 2.8182 to 4.4487. Increased t indicates that rectangles with larger dimensions lead to a stronger localization of electric fields in the space between rectangle and film. At the same time, B monotonically decreases from 0.9931 to −0.2954. Decreased B indicates that rectangles with larger dimensions lead to weaker scattering.

3.2. *Effect of height* b *of rectangle on transmission*

To determine the effect of silver rectangle height b on the transmission characteristics of SPPs on a silver film, b increases from 10 nm to 200 nm with fixed $a = 20$, 40, 60, 80, and 100 nm. When the separation between rectangle and film is zero, SPPs are transmitted from the top surface of the rectangle. When the separation between rectangle and film is greater than zero, SPPs are transmitted not only from the top surface of the rectangle but also from the space between rectangle and film. Figure 3(a) shows the transmittance for $d = 0$ nm. Transmittances dramatically decrease with increased b. A larger b introduces a large reflection and results in small transmittance. Smaller a can transmit both from the top of the rectangle and directly through the rectangle. When b is close to zero, most of the energy is transmitted from the top of the rectangle. With increased b, energy transmitted from the top decreases and energy transmitted through the rectangle increases. This mechanism causes the valley at $b = 56$ nm and the valley at $b = 80$ nm for $a = 40$ nm. Figure 3(b) shows the transmittances for $d = 30$ nm. Similar to Figure 3(a), transmittances dramatically decrease. When $d > 0$, energy transmitted from the space between rectangle and film does not depend on the rectangle size, resulting in the slower decreasing rate in Figure 3(b) compared with that in Figure 3(a). The valleys at small b values of $a = 80$ and 100 nm are due

to the resonance of SPPs in the space between rectangle and film, which satisfies Equation (1) and $N = 1$. In addition, the mechanism of the valley at $b = 168$ nm with $a = 20$ nm is similar to that at $d = 0$, and SPPs have three ways of transmitting energy: the top of the rectangle, the space between rectangle and metallic film, and directly through the rectangle.

3.3. *Effect of width* a *of rectangle on transmission*

To determine the effect of silver rectangle width a on the transmission characteristics of SPPs on metallic film, a is increased from 100 nm to 1200 nm with fixed $b = 20$, 40, 60, 80, and 100 nm. Figure 4(a) shows that for $d = 0$ nm, transmittance periodically varies with increased a. The periods of $b = 20$, 40, 60, 80, and 100 nm are approximately 250 nm. The SPPs propagate along the metallic surface and on the top of the rectangle, with a corresponding SPP wavelength $\lambda_0 = 0.509$ μm. The period is close to half of λ_0, consistent with the momentum-matching relation. For rectangles with smaller b, SPPs are easy to be coupled between the metallic film and the top surface of rectangle, resulting in a larger transmittance. Figure 4(b) shows the transmittance curves with $d = 30$ nm. The transmittances vary in specific periods. The periods of transmittances of $b = 100$ nm obtained by Fourier transform are $P_1 = 730$ nm, $P_2 = 225$ nm, $P_3 = 195$ nm, $P_4 = 154$ nm, and $P_5 = 133$ nm, as shown in Figure 4(c). In the proposed structure, the space between rectangle and film can be considered as a metal–insulator–metal (MIM) waveguide with two ends open to the film. The effective index of the TM_0 mode of the MIM waveguide with $b = 100$ nm is $n_1 = 1.6930 - 0.0114i$ at an excitation wavelength of 0.532 μm. Thus, the wavelength of SPPs in the waveguide is $\lambda_1 = 0.314$ μm. For a larger d, the SPPs propagating on the top of the rectangle are coupled from position A, as shown in Figure 4(d), which is stronger than that of $d = 0$ nm. Thus, the SPPs propagating on the top of the rectangle contribute to the transmission characteristics in Figure 4(b). As aforementioned, the wavelength of SPPs on the top of the rectangle is $\lambda_0 = 0.509$ μm. When resonance occurs around the rectangle, it satisfies $a = N \cdot P$ ($N = 1, 2, 3...$). $P_1 = 3\lambda_0/2 = 5\lambda_1/2$, which is close to the common multiple of the half of λ_0 and the half of λ_1. Thus, the main period in Figure 4(b) is due to the combined contribution of SPPs on the top of the rectangle and the SPPs in the space between rectangle and film. $P_2 = \lambda_0/2$ and $P_4 = \lambda_1/2$, which are due to the resonance of SPPs on the top surface of rectangle and space between rectangle and film, respectively. $P_3 = 2\lambda_0/2 - 2\lambda_1/2$ corresponds to the further increase of a from which the resonance of SPPs between rectangle and film occurs to which the resonance of SPPs on the top of the rectangle appears. $P_5 = 4\lambda_1/2 - 2\lambda_0/2$, which corresponds to the further increase of a from which the resonance of SPPs on the top of the rectangle occurs to which the resonance of SPPs between rectangle and film appears. Periods can be obtained similarly for other b values. Therefore, periods in the transmittance spectra are due to SPP resonance on the top surface of the rectangle, in the space between rectangle and film, or both. When $d > 0$, SPPs are coupled from the bottom of the rectangle. Propagation in the vertical direction generates an additional phase difference affecting the superposition between SPPs from the rectangle top and SPPs from the space between rectangle and film. Additional phase difference decreases with decreased b, which leads to the transmittance increase in Figure 4(b).

4. Conclusions

The effects of silver rectangle on the transmission characteristics of SPPs on a silver film are investigated using the finite-element method. Given the resonances of SPPs on the rectangle and in the space between rectangle and film, transmission valleys occur in the transmission spectra at which enhanced electric fields appear between rectangle and surface. The SPPs are also coupled with the upper facet of the rectangle, where it propagates even for a relatively large distance between rectangle and interface, as well as for a large height of rectangles. The transmission properties of SPPs on silver film are also strongly affected by the structural parameters of the silver rectangle and the separation between rectangle and film. Results reveal that the enhanced electric field caused by the resonance around the rectangle can be applied to enhance nonlinear optics and can help in the applications of SPPs delivery. The coupling mechanism is also suitable for different wavelengths and different substrate materials.

Funding

This work was supported by the National Natural Foundation of China [grant number 11004160]; Fundamental Research Funds for the Central Universities [grant number GK201303007].

References

[1] Barnes, W.L.; Dereux, A.; Ebbesen, T.W. *Nature* **2003,** *424,* 824–830.
[2] Polman, A. *Science* **2008,** *322,* 868–869.
[3] Ozbay, E. *Science* **2006,** *311,* 189–193.
[4] Gay, G.; Alloschery, O.; Lesegho, B.V.D.; O'Dwyer, C.; Weiner, J.; Lezec, H.J. *Nat. Phys.* **2006,** *2,* 262–267.
[5] Takabayashi, M.; Haraguchi, M.; Fukui, M. *J. Mod. Opt.* **1997,** *44,* 119–125.
[6] Zhang, H.F.; Zhang, Z.M.; Guo, Y.; Li, Y.; Bai, L.H. *J. Mod. Opt.* **2014,** *61,* 728–733.
[7] Wang, W.D.; Li, Y.D.; Chen, J.; Chen, Z.Q.; Xu, J.J.; Sun, Q. *J. Mod. Opt.* **2014,** *61,* 1679–1684.

[8] Huang, L.L.; Chen, X.Z.; Bai, B.F.; Tan, Q.F.; Jin, G.F.; Zentgraf, T. *Light Sci. Appl.* **2013,** *2,* e70.
[9] Sun, Q.; Ueno, K.; Yu, H.; Kubo, A.; Matsuo, Y. *Light Sci. Appl.* **2013,** *2,* e118.
[10] Smith, D.R.; Pendry, J.B.; Wiltshire, M.C.K. *Science* **2004,** *305,* 788–792.
[11] Shalaev, V.M. *Nat. Photonics* **2007,** *1,* 41–48.
[12] Anker, J.N.; Hall, W.P.; Lyandres, O.; Shah, N.C.; Zhao, J. *Nat. Mater.* **2008,** *7,* 442–453.
[13] Krasavin, A.V.; Zheludev, N.I. *Appl. Phys. Lett.* **2004,** *84,* 1416–1418.
[14] Li, Q.; Qiu, M. *Opt. Express* **2013,** *21,* 8587–8595.
[15] Dickson, R.M.; Lyon, L.A. *J. Phys. Chem. B* **2000,** *104,* 6095–6098.
[16] Leiβner, T.; Lemke, C.; Jauernik, S.; Müller, M.; Fiutowski, J.; Tavares, L.; Hansen, K.T.; Hansen, J.K.; Magnussen, O.; Rubahn, H.G.; Bauer, M. *Opt. Express* **2013,** *21,* 8251–8260.
[17] Huang, X.P.; Brongersma, M.L. *Nano Lett.* **2013,** *13,* 5420–5424.
[18] Brucoli, G.; Moreno, L.M. *Phys. Rev. B* **2011,** *83,* 075433.
[19] Weeber, J.C.; González, M.U.; Baudrion, A.L.; Dereux, A. *Appl. Phys. Lett.* **2005,** *87,* 221101.
[20] Lamprecht, B.; Krenn, J.R.; Schider, G.; Ditlbacher, H.; Salerno, M.; Felidj, N.; Leitner, A.; Aussenegg, F.R.; Weeber, J.C. *Appl. Phys. Lett.* **2001,** *79,* 51–53.
[21] Polanco, J.; Fitzgerald, R.M.; Maradudin, A.A. *Phys. Lett. A* **2012,** *376,* 1573–1575.
[22] Liaw, J.W.; Wu, P.T. *Opt. Express* **2008,** *16,* 4945–4951.
[23] Hasegawa, K.; Nöckel, J.U.; Deutsch, M. *Appl. Phys. Lett.* **2004,** *84,* 1835–1837.
[24] Bozhevolnyi, S.I.; Volkov, V.S.; Leosson, K.; Erland, J. *Opt. Lett.* **2001,** *26,* 734–736.
[25] Willatzen, M. *Phys. Rev. A* **2009,** *80,* 043805.
[26] Raether, H. *Surface Plasmons on Smooth and Rough Surfaces and on Gratings*; Springer: Berlin, 1988.
[27] Lemke, C.; Leißner, T.; Jauernik, S.; Klick, A.; Fiutowski, J.; Hansen, J.K.; Rubahn, H.G.; Bauer, M. *Opt. Express* **2012,** *20,* 12877–12884.
[28] Mi, G.; Van, V. *Opt. Lett.* **2014,** *39,* 2028–2031.
[29] Kaya, S.; Weeber, J.C.; Zzcharatos, F.; Hassan, K.; Bernardin, T.; Cluzel, B.; Fatome, J.; Finot, C. *Opt. Express* **2013,** *21,* 22269–22284.
[30] Live, L.S.; Bolduc, O.R.; Masson, J.F. *Anal. Chem.* **2010,** *82,* 3780–3787.
[31] Schwind, M.; Kasemo, B.; Zorić, I. *Nano Lett.* **2013,** *13,* 1743–1750.
[32] Rotenberg, N.; Spasenovie, M.; Krijger, T.L.; Feber, B.L.; Garcia da Abajo, F. J.; Kuipers, L. *Phys. Rev. Lett.* **2012,** *108,* 127402.
[33] Arias, R.E.; Maradudin, A.A. *Opt. Express* **2013,** *21,* 9734–9756.
[34] Sánchez-Gil, J.A. *Appl. Phys. Lett.* **1998,** *73,* 3509–3511.
[35] Lindquist, N.C.; Jose, J.; Cherukulappurath, S.; Chen, X.; Johnson, T.W.; Oh, S.-H. *Laser Photonics Rev.* **2013,** *7,* 453–477.
[36] Ruan, Z.C.; Wu, H.; Qiu, M.; Fan, S.H. *Opt. Lett.* **2014,** *39,* 3587–3590.
[37] Bar-Lev, D.; Arie, A.; Scheuer, J.; Epstein, I. *J. Opt. Soc. Am. B* **2015,** *32,* 923–935.
[38] Min, C.; Wang, P.; Jiao, X.; Deng, Y.; Ming, H. *Appl. Phys. B* **2008,** *90,* 97–99.
[39] Bohren, C.F., Huffman, D.R., Eds.; *Absorption and Scattering of Light by Small Particles*; Wiley-Interscience: New York, **1983;** pp 63–68
[40] Johnson, P.B.; Christy, R.W. *Phys. Rev. B* **1972,** *6,* 4370–4379.